Nano Energy 51 (2018) 10–18

Contents lists available at ScienceDirect

Nano Energy

journal homepage: www.elsevier.com/locate/nanoen

Full paper

Progressive contact-separate triboelectric nanogenerator based on conductive polyurethane foam regulated with a Bennet doubler conditioning circuit

Hemin Zhang[a], Yingxian Lu[a], A. Ghaffarinejad[a,b], Philippe Basset[a,*]

[a] Université Paris-Est, ESYCOM, ESIEE Paris, BP 99, 2 bd Blaise Pascal, 93162 Noisy-le-Grand Cedex, France
[b] School of Electrical Engineering, Iran University of Science and Technology, Tehran 16846-13114, Iran

ARTICLE INFO

Keywords:
Triboelectric nanogenerator
Conductive polyurethane foam
Energy harvesting
Bennet doubler conditioning circuit

ABSTRACT

Scavenging the energy of human motions has attracted widespread attentions with the development of wearable electronics. This paper for the first time proposed a progressive triboelectric nanogenerator based on macro-triangle-prism-shaped conductive polyurethane (PU) foam and polytetrafluoroethylene (PTFE) film, which occupy the top and bottom spots of the triboelectric table respectively. The proposed macro-structured conductive PU foam also integrates the functions of spring, spacer and electrode. Thanks to the innovative structures and chosen of the materials, an extended current pulse width is obtained. A maximum RMS power density of 100 nJ/cm^2/tap was obtained with a 60 MΩ resistive load and press force of 10 N@5 Hz. By regulating the TENG with a Bennet doubler conditioning circuit, the ubiquitous voltage saturation phenomenon when charging a storage capacitor using full-wave rectifiers is avoided. Moreover, the energy per cycle, charging efficiency and totally stored energy can be exponentially pumped up. With a Bennet circuit charging a 5 nF capacitor, a harvested energy density of ~ 710 nJ/cm^2/tap was obtained when voltage across the capacitor was 400 V. Putting the device under sole within 25 human steps, the totally stored energy was 0.43 mJ with a Bennet circuit, 3.6 times higher than that using a full-wave rectifier (0.12 mJ). The Bennet was proven better for regulating the triboelectric nanogenerators with long operation-time compared to the classical full-wave rectifier.

1. Introduction

There is a continuously growing demand for new power sources with the rapid development of flexible electronics and wireless sensing nodes for applications in medical and structural health monitoring, internet of things (IoT) and environmental sensing [1–5]. The most commonly used power, i.e. chemical battery, is always accompanied with a limited lifetime and environmental problems [6]. The nanogenerator, which transduces environmentally existing energy including solar, thermal, mechanical and chemical energy to electricity, is a remarkable solution due to its renewable, flexible and sustainable properties [7]. Among different environmental energy sources, mechanical energy from vibrations, body motion, water/acoustic waves and even wind flow, is widely distributed and relatively easy to be harvested for the applications of wearable electronics. Therefore, emerging techniques including piezoelectric [8–10] and triboelectric-electret nanogenerators (TENG) [11–19] attract a wide attention, owing to the possibility of developing high-efficiency, flexible, biocompatible, and environmentally friendly mechanical energy harvesting devices. TENGs are particular electrostatic kinetic energy harvesters (e-KEH) [20] based on the coupling of contact electrification and electrostatic induction. Among four basic working modes [11] of TENG, the contact-separate (CS) mode is mostly concerned because of its high-efficiency and wide range of application [21]. CS-TENG consists in physical contact of two materials with different abilities of attracting electrons. Opposite charges are left on the surfaces of the two friction materials, and a current will take place from one electrode to another to rebalance the electrostatic field when they contact/separate each other with mechanical force, as for any e-KEH.

The output performances of TENG can be improved by enlarging the surface area [22], increasing the surface charge density [23,24], or adding 2-dimensional materials as charge store layers [25]. However, least attentions were paid to the elastic part of the TENG, although it is of great significance for the output performances. The material properties and structural designs of the mechanical springs define the contacting time, the approaching and detaching velocity, and the separating gap of the two electrodes, all these three points being crucial for a TENG. Various spring designs and materials have been tested including

* Corresponding author.
E-mail address: philippe.basset@esiee.fr (P. Basset).

https://doi.org/10.1016/j.nanoen.2018.06.038
Received 4 May 2018; Received in revised form 4 June 2018; Accepted 10 June 2018
Available online 15 June 2018

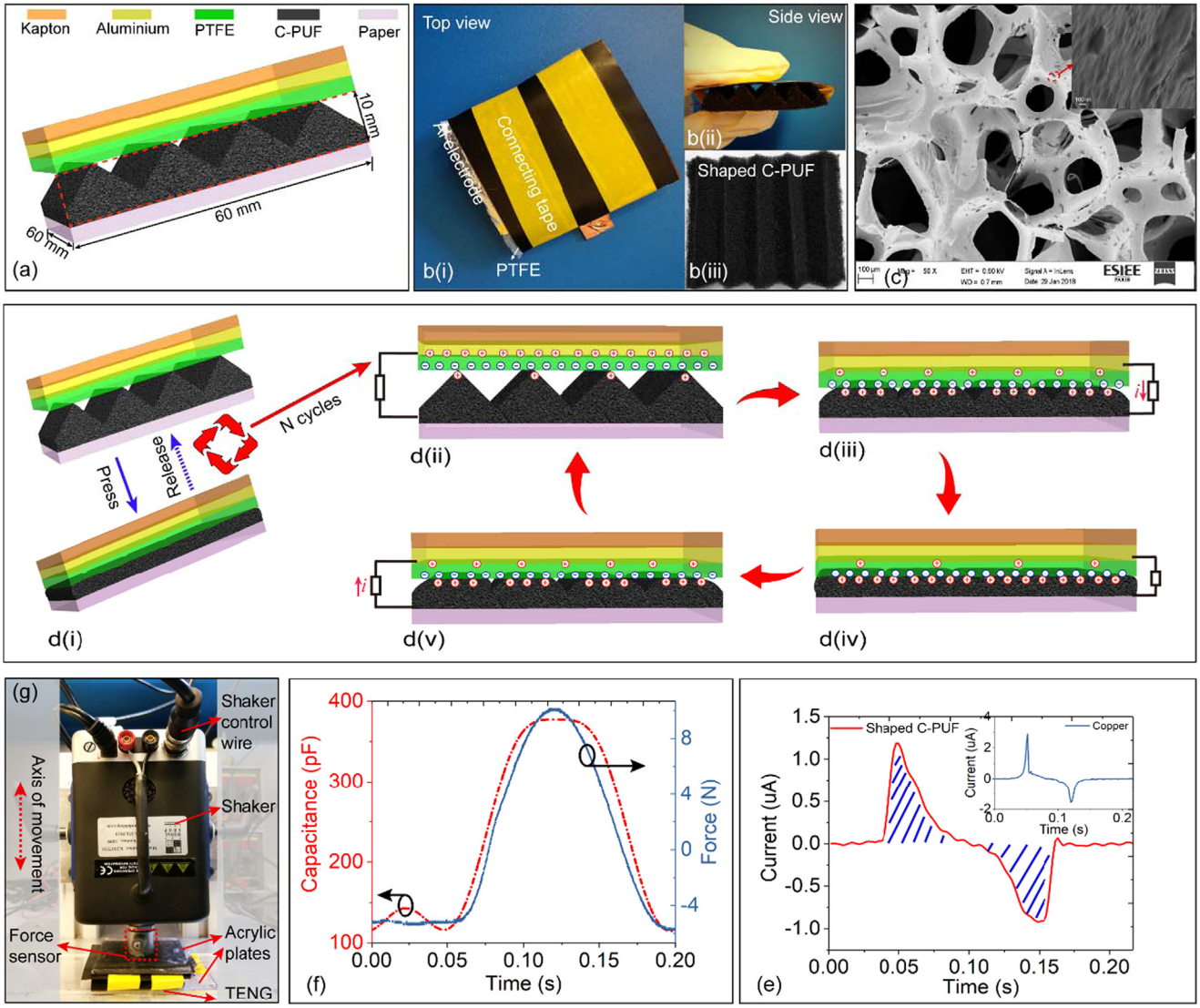

Fig. 1. Illustration and principles of the fabricated TENG. Diagram of the TENG (a). Top view b(i), side view b(ii), and fabricated C-PUF with triangle prisms b(iii). SEM image of the C-PUF (c). Process of the electron transport between different layers during operation (d). Measured transient current of the TENG (e), the inset figure is the current of a TENG using planar copper and PTFE as the friction materials. Capacitance variation of the TENG (e). Measurement setup (g).

classical metal spring [15], flexible polymer such as Kapton [26], arched or wave-shaped structures integrated with electrodes [14,27,28], and flat foam [29] as spacers to separate the two friction layers. However, the above designs have the drawbacks of wasting spaces and/or being sometimes not fully flexible. More advanced structure designs allow to enhance the electrical performances and application practicality of the TENG, for instances the bellows-type [17] that includes the packaging of the TENG, multilayers stacked silicone elastomers [30], and paper-cutting structures [31,32]. Interestingly, we noted that no researchers selected the commercial available low-cost open-cellular polyurethane (PU) foam as the spring materials except [29] utilizing flat PU foam as a spacer. In addition to the high shape recovery property of the PU foam, which gives it the potential to be a good spring, the PU foam is also a good friction layer since it occupies the top spot of positive materials in the triboelectric table [11]. The only time PU foam was used as the friction material was reported in [33].

In this paper, the authors propose a novel TENG based on a macro-structured *conductive PU foam* (C-PUF), which is PU foam doped with conductive carbon black powder, and a polytetrafluoroethylene (PTFE) film that is close to the bottom of the triboelectric table [11]. The C-PUF was shaped into macro scale triangle prisms, while its porous surface has micro/nano 3D structures. At the same time, C-PUF plays the roles of spring, spacer, friction layer and electrode. To the best knowledge of the authors, this is the first time that a conductive foam, and in particular C-PUF, is used for TENG in such a way: thanks to the macro-triangle prism shape, the contact and separation between the two electrodes become progressive. This means that the friction area is gradually growing/decreasing as the external force is applied/released. In this way the device operates as a mix between the contact-separation and the sliding modes. Due to its innovative structures and the chosen materials, the TENG gets the property of self-release without using extra springs. As it will be shown in the next section, the area below the current curve (that is directly related to the width of the current peak and to the harvested energy) is highly extended because the contacting time between the two friction materials are greatly enhanced thanks to the progressive contact and separate actions. The proposed TENG is particularly suitable for practical applications such as energy harvesting and pressure sensing for in/under sole during human walking. In addition, we also experimentally demonstrate that the universal voltage saturation phenomenon when charging a capacitor with a full-wave rectifier within a certain operation cycles can be avoided by using a Bennet doubler conditioning circuit [34–36]. The Bennet doubler

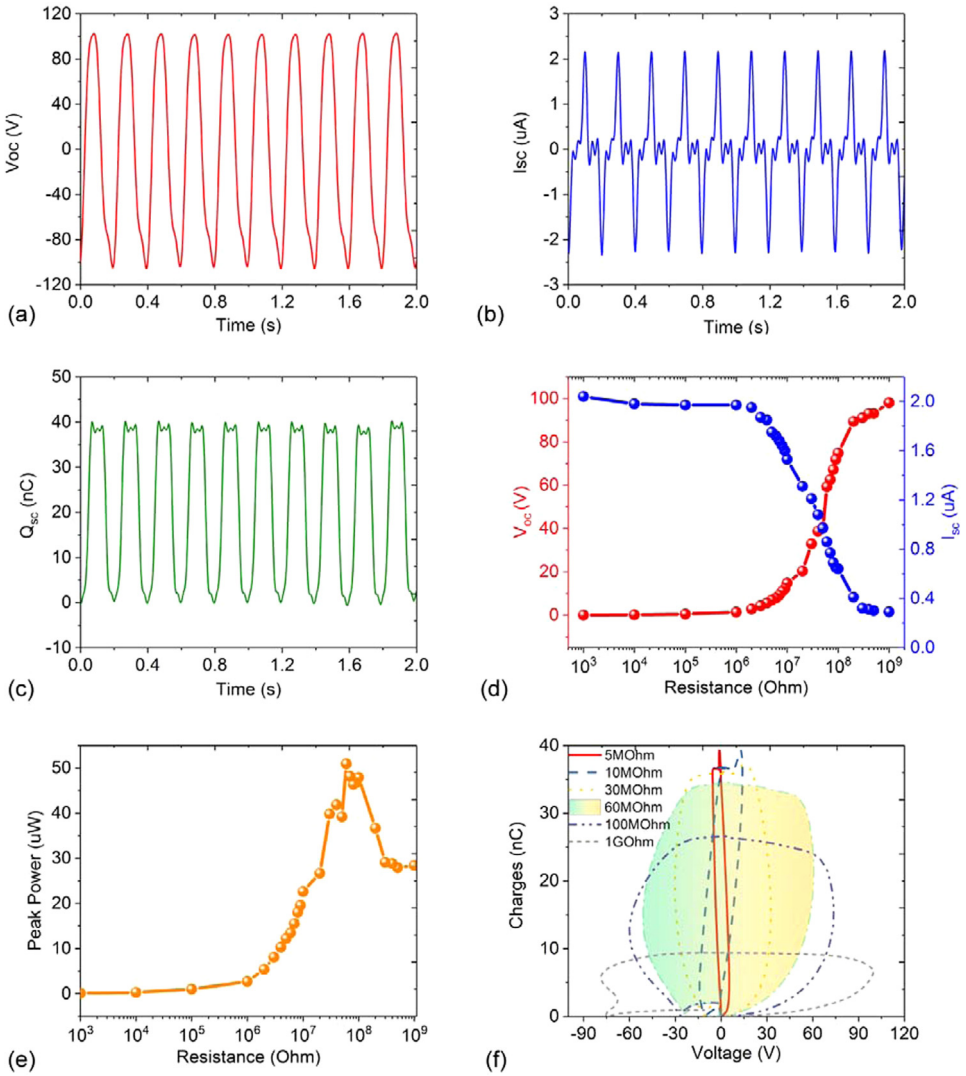

Fig. 2. Electrical characterization of the TENG with a resistive load. Open-circuit voltage (a), short-circuit current (b), and transferred charges in short circuit mode of the TENG (c). TENG peak current/voltage (d). Converted power (e) versus load resistance. TENG QV cycles with different load resistance (f).

conditioning circuit also leads to a considerable improvement on the harvested energy per cycle and charging efficiency.

2. Experimental section

2.1. Comparison of materials

We first compared the output performances of a basic contact separation TENG using planar un-conductive PU foam (UC-PUF), copper or C-PUF (from Shanghai Leenol Industrial Co., Ltd) as the positive friction materials. The PU foams are fabricated with ~ 60–65% polyol/polyester resin, ~ 25% TDI (toluene-2, 4-diisocyanate), and ~ 5–10% water-soluble resin. In addition, the C-PUF is doped with ~5% conductive carbon black powder. The density of both PU foam is ~ 25 kg/m^3. The surface resistivity of the C-PUF is 10^3–10^6 Ω/sq, while that of the UC-PUF is > 10^{12} Ω/sq. The testing setup and results are shown in Supplementary material (note 1 and Fig. S1). The output peak voltage of the C-PUF-based TENG with 100 MΩ load is ~ 46 V, while that of the TENG with copper and UC-PUF are ~ 36 V and ~ 12 V, respectively. UC-PUF had poor performances compared to C-PUF because the large thickness of the UC-PUF (5 mm) severally limits the available maximum capacitance $C_{max(foam)}$, the capacitance variation of the TENG and then the energy transduction. This maximum capacitance is given by:

$$C_{max\ (foam)} = \frac{\varepsilon_{eff} S_{eff}}{d_{PTFE} + d_{foam}} \quad (1)$$

where ε_{eff} is the effective permittivity of dielectrics between the electrodes, S_{eff} is the effective surface area of the overlapping electrodes, d_{PTFE} and d_{foam} are the thicknesses of PTFE and PU foam in full compression respectively. However, because of the conductive carbon black power inside of the C-PUF, the gap d_{foam} almost disappeared and thus the output is much higher. In addition, because of its rough surface that created higher friction, the C-PUF TENG gets better results than flat copper.

2.2. Fabrication of the TENG

A schematic of the proposed TENG is shown in Fig. 1a. First, an aluminium electrode with a dimension of 60 mm × 60 mm × 100 μm was pasted to an insulating Kapton substrate. Then a PTFE film of 50 μm was sticked to the aluminium electrode, as the negative friction layer. The second electrode of the device was fabricated using the C-PUF with initial thickness of 10 mm, manually shaped with 5 triangle prisms. The C-PUF was sticked to a paper substrate. Pictures of the TENG are shown in Fig. 1b including its top view, side view and shaped C-PUF. A SEM image of the C-PUF is shown in Fig. 1c. The PTFE film is a little larger (65 × 65 mm^2) than the aluminium to make sure that

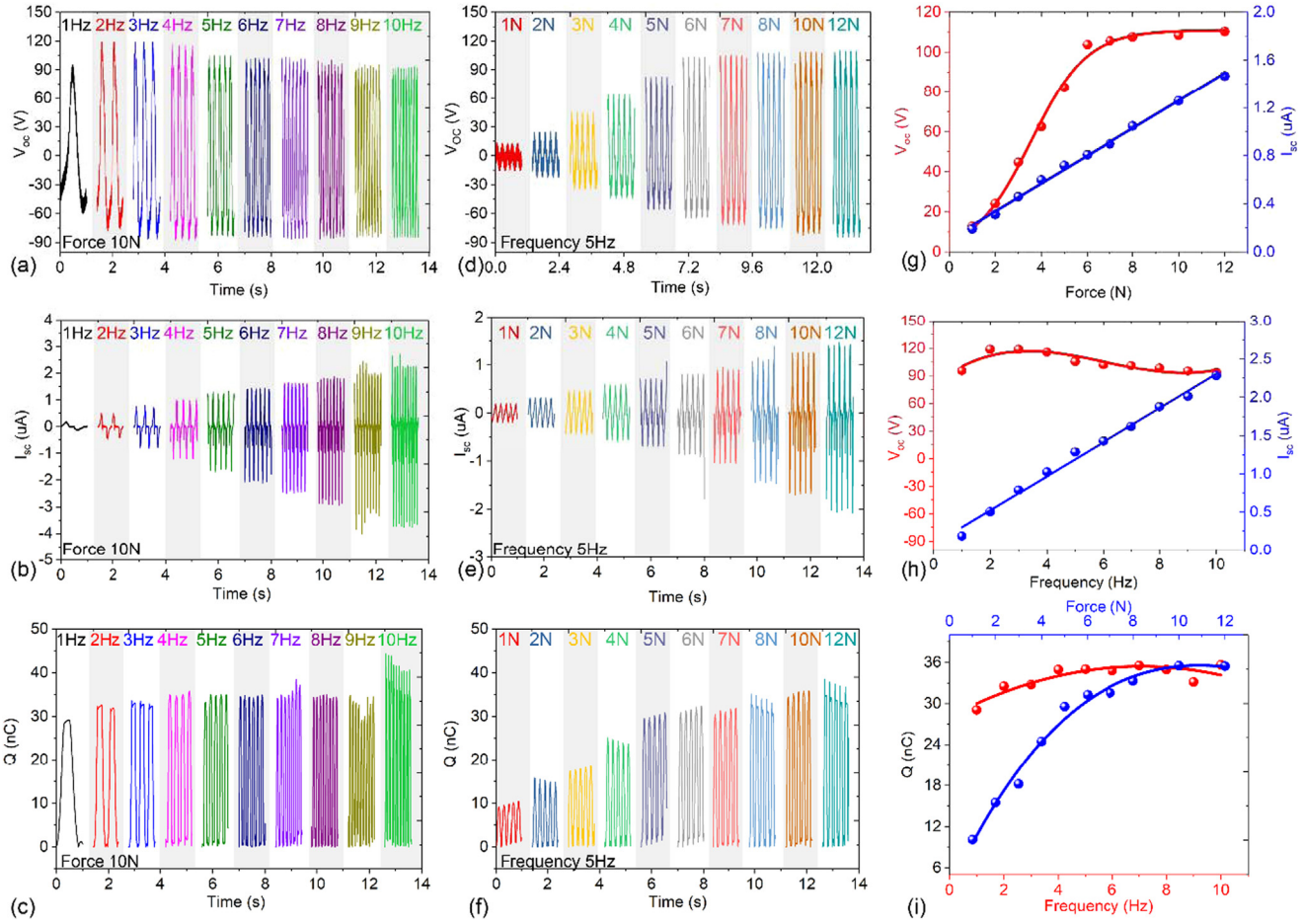

Fig. 3. Electrical characterizations of the TENG under different press forces and frequencies. Open-circuit voltage (a), short-circuit current (b) and transferred charges (c) of the TENG versus frequency with a constant force of 10 N. Open-circuit voltage (d), short-circuit current (e) and transferred charges (f) of the device versus press force with a frequency of 5 Hz. (g) Peak values of the open-circuit voltage and short-circuit current as functions of the frequency. (h) Peak values of the open-circuit voltage and short-circuit current as functions of the press force. (i) Transferred charges in short-circuit mode as the functions of the frequency and force.

there is no short circuit between the aluminium electrode and the C-PUF electrode during operation of the TENG.

2.3. Experimental setup

The fabricated device was placed under a vibration shaker (MODAL SHOP K2007E01), where the vibration frequency and amplitude/force can be controlled with a signal generator (Tektronix AFG3102). The mechanical setup of the shaker is shown in Fig. S2a, and its picture is shown in Fig. 1g. The applied force was measured using a force sensor. The output voltage of the device was measured with a digital oscilloscope (LeCroy 9354AL) at the output of a voltage follower. The current was measured with a picoammeter (Keithley 6485), and recorded through GPIB on a PC. Signal rectification was obtained with a full-wave rectifier or a Bennet doubler conditioning circuit, using low-leakage diodes having a reverse voltage of ~ 250 V. The TENG capacitance variation was measured using the technique in [37]. The capacitance variation of the device during press and release is shown in Fig. 1f, indicating a capacitance variation of ~ 3 with a peak force of 10 N.

3. Results and discussions

3.1. Working principle

The operation process of the TENG is shown in Fig. 1d(i)–(v). After a transitory regime (Fig. 1d(i)) where the PTFE triboelectric-electret layer will be charged at its saturation level [38], the surface of the PTFE and C-PUF will be distributed with negative and positive charges respectively (Fig. 1d(ii)), due to the tendency of PTFE to gain electrons and C-PUF to lose electrons. Due to the original macro-shape of the C-PUF, when the device is pressed, the contact (or friction) surface area between PTFE and C-PUF increases progressively. At the same time the gap between the aluminium and the C-PUF electrodes decreases (Fig. 1d(iii)), then the transducer's capacitance increased. Simultaneously, a current is flowing from the aluminium electrode to C-PUF until C-PUF is fully pressed (Fig. 1d(iv)), corresponding to the TENG maximum capacitance. In contrast, the contact surface area and TENG capacitance progressively decreases while releasing the pressure on the shaped C-PUF, leading to an opposite current until the C-PUF is fully released (Fig. 1d(v)–(ii)). The measured transient current is shown in Fig. 1e. It has noted that this current is not like the current transient response of the traditional contact-separate TENG with solid-solid contact [14–17] that is always accompanied with thin and tall peaks (shown by the inset in Fig. 1e where copper is used). It is more like the TENG with solid-fluid contact that shows a much wider pulse width [39]. This is due to the high friction time between PTFE and the triangular prism shaped C-PUF caused by the progressive contact. Even if the maximum value of the current peak is smaller, its width is greatly improves. It corresponds to an increase of the root means square (RMS) current, which is the only relevant value in terms of energy conversion [36].

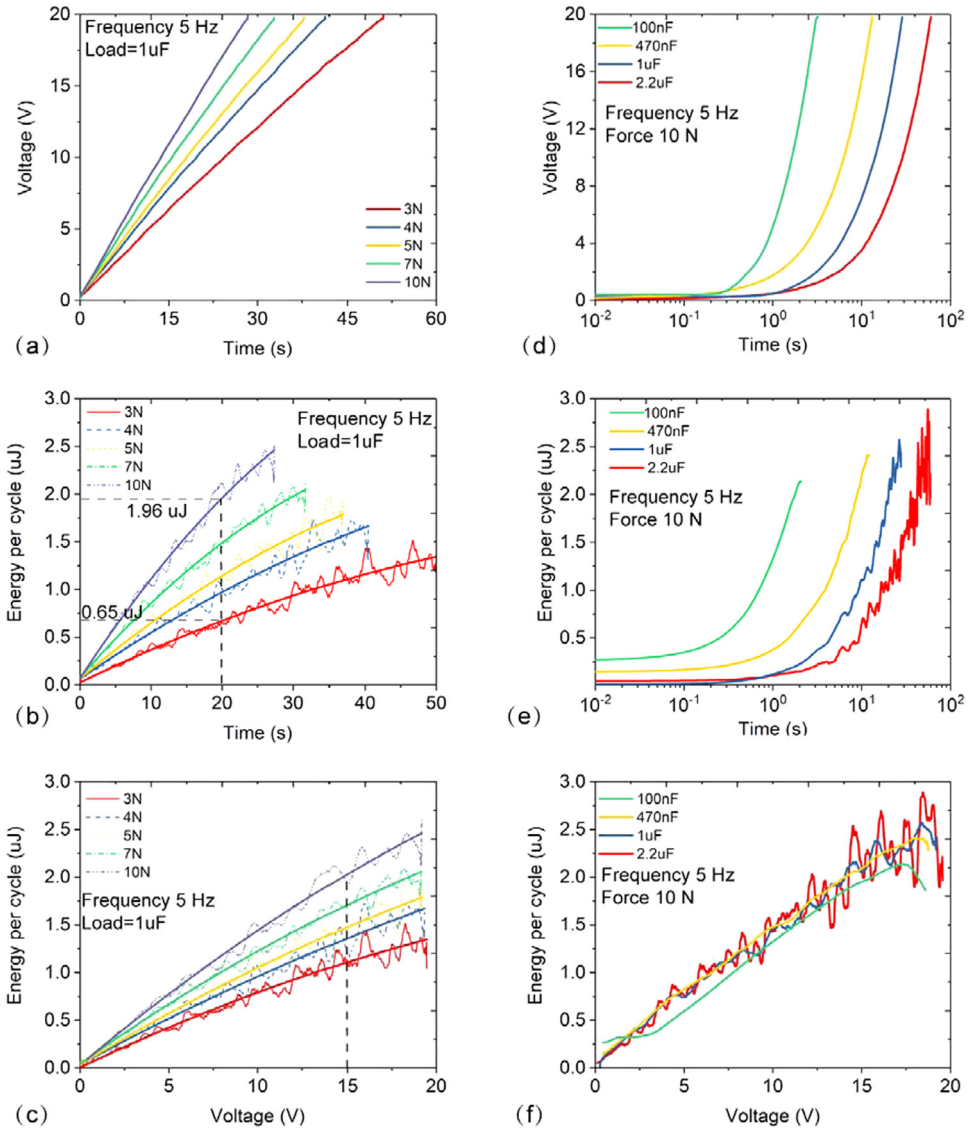

Fig. 4. Electrical characterization of the TENG with a full-wave rectifier. Voltage of the storage capacitor (1 μF) versus time (a), energy per cycle versus time (b) and energy per cycle versus voltage (c) under different press forces with a constant frequency of 5 Hz. Voltage of the storage capacitor (d), energy per cycle versus time (e) and energy per cycle versus voltage (f) with different values of capacitances under a press force of 10 N@5 Hz.

3.2. Power delivery with resistive loads

In order to characterize the TENG, we first connected it to a resistive loads and we used the vibration shaker to press the device with a maximal force of 10 N and a frequency of 5 Hz. The open-circuit voltage is obtained with a resistive load of 6 GΩ, and the electrical setup is shown in Supplementary material Fig. S2b. The peak values of the open-circuit voltage and short-circuit current are 102 V and 2.2 μA respectively, as depicted in Fig. 2a and b. The transferred charges (Fig. 2c) are calculated based on the time integration of the current: $Q_{t_0} = \int_0^{t_0} idt$. The peak voltage and current of the TENG with variable resistive load are shown in Fig. 2d, and the electrical measurement setup is shown in Supplementary material Fig. S2c. The maximum instantaneous power appears at the optimized load of 60 MΩ (shown in Fig. 2e) and is equal to 53 μW, corresponding to a power density of ~ 1.5 μW/cm^2. More important, the RMS power density is ~ 0.52 μW/cm^2, corresponding to 100 nJ/cm^2/tap and to 3.7 μJ per tap for the full device.

The *QV* cycle (charges versus voltage) is an intuitive geometrical tool to describe the operation of any electrostatic energy harvester [20]. It allows a quick calculation of the amount of the converted energy during one cycle of the transducer's capacitance variation using simple geometric arguments: the converted energy in a given cycle is equal to the area enclosed by the *QV* loop for this cycle [13,40,41]. As shown in Fig. 2f, the area of the *QV* cycle gets the maximum at the resistive load of 60 MΩ, which perfectly matches the optimized instantaneous peak power in Fig. 2e.

TENGs are usually used to scavenge the low-frequency environmental energy by direct applied pressure. Thus frequency and force responses of the TENG have been investigated. The transient open-circuit voltage, short-circuit current and transferred charges (in short circuit mode) of the device versus frequency with a force of 10 N were recorded in Fig. 3a–c respectively. The peak values of the open-circuit voltage and short-circuit current versus frequency are summarized in Fig. 3g. The open-circuit voltage is more or less constant around 100 V (it reaches a maximum at 2 Hz with a peak value of 120 V, and the minimum peak voltages from 1 Hz to 10 Hz are larger than 95 V). The transferred charges in short circuit mode (shown in Fig. 3i) are also not very sensitive to the frequency, on the contrary to the short-circuit current that operates as a linear function.

With the frequency fixed to 5 Hz, the open-circuit voltage, short-circuit current and transferred charges of the TENG were recorded with

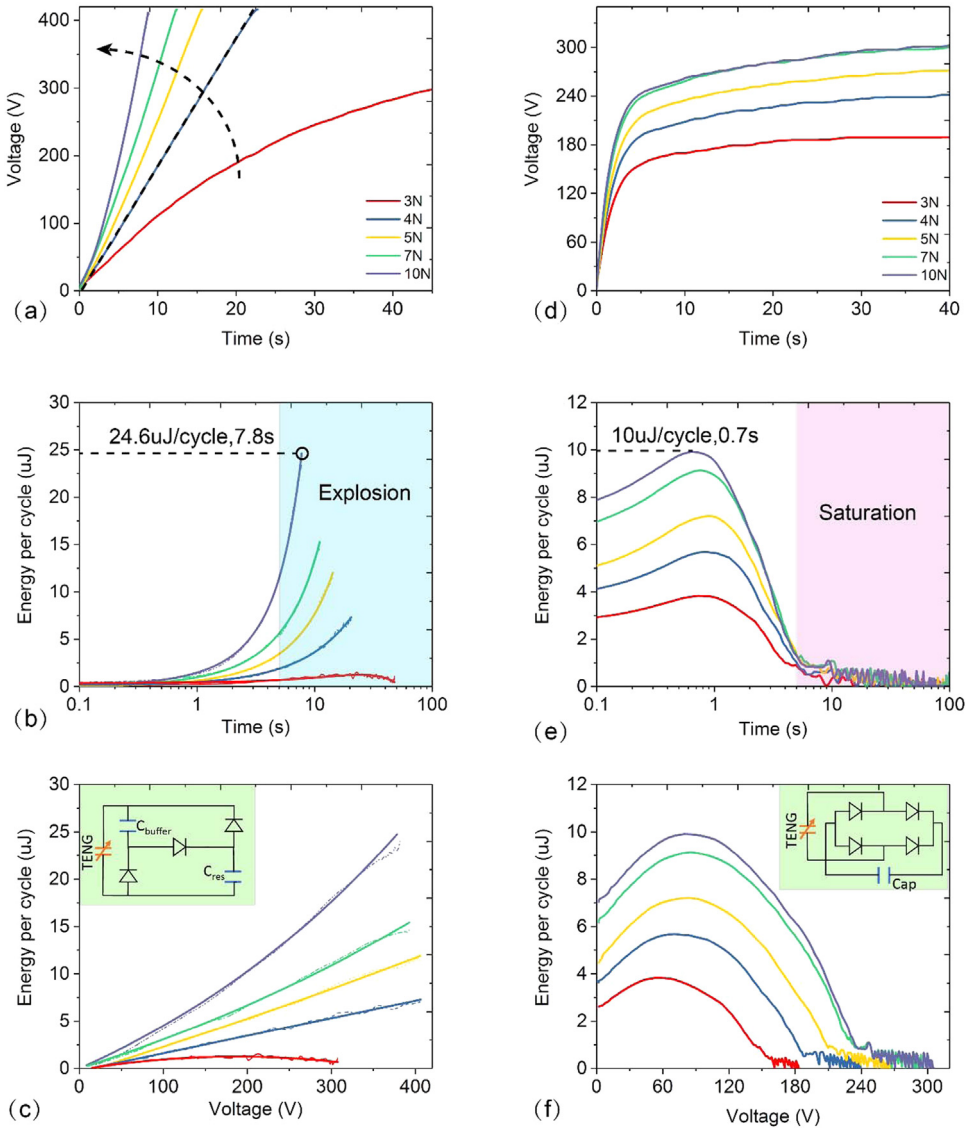

Fig. 5. Electrical characterizations of charging a capacitor with a Bennet circuit and a full-wave rectifier with a constant frequency of 5 Hz. Voltage of C_{res} (a), energy per cycle of C_{res} versus time (b), and energy per cycle of C_{res} versus voltage (c) under Bennet circuit with different press forces. Voltage of C_{ap} (d), energy per cycle of C_{ap} versus time (e), and energy per cycle of C_{ap} versus voltage (f) under full-wave rectifier with different press forces. The inset figures in (c) and (f) are the brief schematics of Bennet and full-wave circuit.

the variation of the applied press force and shown in Fig. 3d–f respectively. The peak values of the open-circuit voltage and short-circuit current as functions of the force are summarized in Fig. 3h. The peak voltage raises up when increasing the force until the force reaches 8 N. After then, the peak voltage do not increase, no matter the value of the force. This is because the capacitance variation achieves its maximum around 8 N. The transferred charges versus forces in short circuit mode perform similarly, as shown in Fig. 3i. In contrast, the short-circuit current is linearly growing with the increasing force, as shown in Fig. 3h. The reason is that a larger force causes a faster press-release cycle, while the stiffness and deformation of the C-PUF are kept constant.

3.3. Power delivery with a full-wave rectifier

A 1 μF capacitor was charged through a full-wave rectifier, and the voltage of the storage capacitor was monitored with a follower (electrical measurement setup can be found in Supplementary material Fig. S3a). Output voltages versus various applied forces on a 1 μF capacitor and a fixed frequency of 5 Hz are shown in Fig. 4a. As expected, the slope of the charging curve is increasing with a larger force. The total accumulated energy after n cycles is calculated based on:

$$E_{tot} = C_{res} V_n^2/2 \quad (2)$$

where C_{res} is the storage capacitor. The converted energy per cycle, which represents the stored energy during one press-release cycle, is another important factor to judge the performance of the TENG [35]. It can be extracted from:

$$\Delta E_{cyc} = C_{res}(V_{n+1}^2 - V_n^2)/2 \quad (3)$$

V_{n+1} and V_n meaning the voltage across C_{res} after $n + 1$ and n cycles respectively. Fig. 4b shows the energy per cycle growing up with time. The energy per cycle is progressively reaching a saturated value since the tangent slope is getting smaller and smaller with time. After 100 taps (20 s), the energy per cycles are 0.65 μJ/cycle at 3 N and 1.96 μJ/cycle at 10 N. The converted energy per cycle versus the voltage across C_{res} is shown in Fig. 4c. As for any e-KEH, the higher the voltage on Cres, the higher the converted energy per cycle. When the capacitor voltage reaches 15 V, the energy per cycles are 1.11 μJ/cycle at 3 N

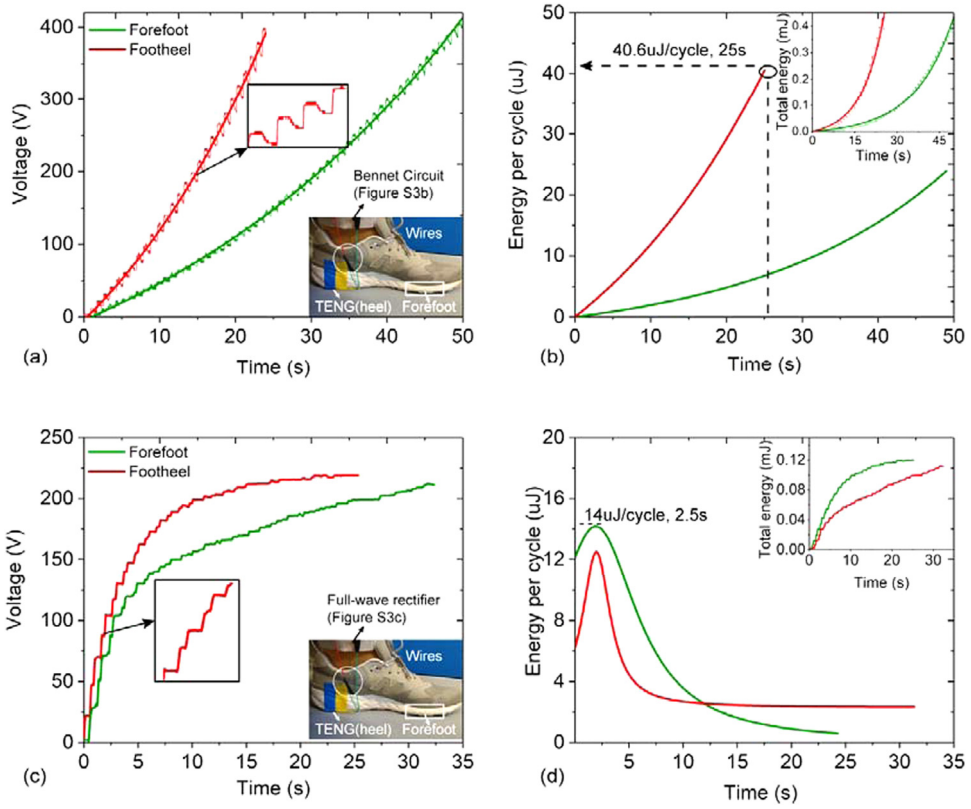

Fig. 6. Output voltage of the capacitor (a) and energy per cycle versus time (b) with Bennet circuit; output voltage of the capacitor (c) and energy per cycle versus time (d) with full-wave rectifier. The inset figures in (b) and (d) are the corresponding total storage energy.

after 190 taps and 2.02 μJ/cycle (~ 56 nJ/cm^2/tap) after 100 taps at 10 N. Concerning the effect of the frequency, the capacitor voltage, energy per cycle versus time and voltage are shown in Supplementary material (Fig. S4).

Similarly as for resistive loads, the capacitive load should be carefully chosen [42] for TENG. Therefore, here we studied the charging performance of the TENG with variable capacitors. Fig. 4d–f show the voltage, energy per cycle versus time and voltage with variable capacitances respectively. For sure, when capacitance increases, the time to get a certain value of energy per cycle is going up. What's interesting is that the energy per cycle is growing faster with a smaller capacitor. And with the same voltage, the capacitor gets almost the same energy per cycle seen from Fig. 4f. The totally stored energy versus time with different capacitance is shown in Supplementary material Fig. S5. It is obtained that a smaller capacitance is faster than a larger one to store the same energy.

3.4. Power delivery with a Bennet doubler

As it can be seen in the above results and many other previous works [43,44], the output voltage of diode-bridge rectifiers is limited to the output voltage of the TENG, which is equivalent to a saturation phenomenon. We recently proposed to use a Bennet doubler conditioning circuit with TENGs [34], which increases the voltage across the storage capacitor exponentially to an ultra-high value [45]. Limitations can come from the spring-softening effect in inertial e-KEH [20], the diode reverse current and the diode Zenner voltage [35], or even the air breakdown according to the Paschen law.

In this section, a Bennet doubler conditioning circuit is used to rectify the TENG output voltage. The setup of the Bennet circuit is described in the Supplementary material (Fig. S3b). The voltages across C_{res} versus time and for various applied forces with the Bennet doubler circuit are shown in Fig. 5a. When the force is larger than 5 N, the losses in the circuit become negligible and the output voltage tends to increase as an exponential function. The reason why the exponential increase appears only with larger forces, is because the Bennet doubler requires a capacitance variation larger than 2 [41], which can hardly be fulfilled with a small press force. Voltage across C_{res} reaches 400 V within less than 8 s, and the voltage can be even higher with time. As a comparison, a full-wave rectifier with a capacitor divider was also studied and the setup is shown in Supplementary material (Fig. S3c). The voltage across C_{res} gets to a saturated voltage of ~ 260 V within 5 s with the full-wave rectifier, as shown in Fig. 5d. By comparing the energy per cycle versus time between Bennet circuit and full-wave rectifier in Fig. 5b and e, it can be concluded that the converted energy per cycle with the Bennet doubler circuit is always increasing unless the conditions mentioned above are reached (strong electro-mechanical coupling, diode losses or dielectric breakdown), while that with full-wave rectifier is first increasing to a peak value and then quickly drops progressively to zero when the output voltage across C_{res} reaches the voltage across the TENG. When press force is set to 10 N at 5 Hz, the energy per cycle reaches 25.6 μJ/cycle (128 μW) within 7.8 s with the Bennet doubler circuit, while the peak value of energy per cycle using the full-wave rectifier is 10 μJ/cycle (50 μW) at 0.7 s.

Furthermore, with a larger storage capacitor, such as a 0.1 μF capacitor (C_{res1} in Fig. S3(b)) in parallel with a 2 μF capacitor (C_{res2} in Fig. S3(b)), corresponding to a storage capacitance of 0.095 μF, the performances of the Bennet doubler and the full-wave rectifier were compared (see Supplementary material Fig. S6). The results indicate that the Bennet doubler has better charging performance in case the operation time is long and the voltage is high, while the full-wave rectifier does better at the initial or the low-voltage stages.

3.5. Energy harvesting under sole

In this section, we placed the TENG under a sole to evaluate its

performance for human walking energy harvesting. The tests were performed with both Bennet doubler and full-wave circuits, and the electrical schematics are shown in Supplementary material Fig. S3b and c respectively. The step frequency is 1 Hz. With the Bennet doubler, the converted energy achieves 40.6 μJ/cycle within 25 s (25 steps), corresponding to a harvesting power of 40.6 μW when the TENG was put under the footheel. When the TENG was put under the forefoot, it achieves 24.1 μJ/cycle within 48 steps. In comparison, the energy per cycle using a full-wave rectifier is limited to 14 μJ/cycle (footheel) after 2.5 s, as shown in Fig. 6d. The total harvested energy using the Bennet doubler under footheel is 0.43 mJ within 25 steps (see the inset in Fig. 6b), while it is only 0.12 mJ with full-wave rectifier as shown in the inset in Fig. 6d. Thus, within 25 steps the total harvested energy using the Bennet doubler is almost 3 times better than with the full-wave rectifier.

4. Conclusions

In summary, a progressive contact-separate TENG based on macro-shaped and commercially supplied conductive polyurethane foam was demonstrated. Its electrical characterizations with resistive loads and power delivery with capacitive loads regulated with a full-wave rectifier or a Bennet circuit were studied. The macro-structured C-PUF with triangle prisms plays the roles of spring, spacer, friction material and also electrode. A maximum converted energy density of ~ 100 nJ/cm^2/tap with a 60 MΩ resistive load as a conditioning circuit is achieved when press force is 10 N@5 Hz. With a full-wave diode bridge circuit on a 1 μF capacitor, a harvested energy density of ~ 56 nJ/cm^2/tap was achieved when the voltage across the capacitor was 15 V after 100 taps. With a Bennet doubler circuit on a 5 nF capacitor, a harvested energy density of ~ 710 nJ/cm^2/tap was obtained when voltage across the capacitor was 400 V after 40 taps.

It was proven that the Bennet doubler conditioning circuit is much better to be used for TENG in the situation with long-time operations. These demonstrations provide another possible structure design, material and conditioning circuit for TENGs. However, the resistivity of the C-PUF is not as good as the metal electrode, which limits the output current of the device. Therefore, it is better to fabricate conductive PU foam doped with carbon nanotube, to enhance the conductivity of the foam. A drawback of using the Bennet circuit is the starting time or initial time is with low charging efficiency, and the final voltage of the storage capacitor is so high making the following circuit complicated for matching the voltage limitation of any electronics. In the future work, we will focus on lowering the voltage of the storage capacitor based on Bennet circuit while keeping its charging efficiency.

Acknowledgement

We really appreciate Prof. Dimitri Galayko, Sorbonne Universités, for the discussions on Bennet circuit.

Appendix A. Supplementary material

Supplementary data associated with this article can be found in the online version at http://dx.doi.org/10.1016/j.nanoen.2018.06.038.

References

[1] E.B. Secor, S. Lim, H. Zhang, C.D. Frisbie, L.F. Francis, M.C. Hersam, Adv. Mater. 26 (2014) 4533–4538.
[2] D. Son, J. Lee, S. Qiao, R. Ghaffari, J. Kim, J.E. Lee, C. Song, S.J. Kim, D.J. Lee, S.W. Jun, S. Yang, Nature 9 (2014) 397–404.
[3] S.-K. Kang, R.K. Murphy, S.-W. Hwang, S.M. Lee, D.V. Harburg, N.A. Krueger, J. Shin, P. Gamble, H. Cheng, S. Yu, Nature 530 (2016) 71–76.
[4] H. Zhang, B. Li, W. Yuan, M. Kraft, H. Chang, J. Microelectromech. Syst. 25 (2016) 286–296.
[5] K. Tao, L.H. Tang, J. Wu, S.W. Lye, H.L. Chang, J.M. Miao, J. Microelectromech. Syst. 27 (2018) 276–288.
[6] D. Larcher, J.M. Tarascon, Nat. Chem. 7 (2015) 19–29.
[7] F.R. Fan, W. Tang, Z.L. Wang, Adv. Mater. 28 (2016) 4283–4305.
[8] Z.L. Wang, J. Song, Science 312 (2006) 242–246.
[9] K.Y. Lee, D. Kim, J.H. Lee, T.Y. Kim, M.K. Gupta, S.W. Kim, Adv. Funct. Mater. 24 (2014) 37–43.
[10] L. Serairi, L. Gu, Y. Qin, Y. Lu, P. Basset, Yamin Leprince-Wang, Eur. Phys. J. – Appl. Phys. 80 (2017) 30901.
[11] J. Chen, Z.L. Wang, Joule 1 (2017) 480–521.
[12] F.R. Fan, Z.Q. Tian, Z.L. Wang, Nano Energy 1 (2012) 328–334.
[13] S. Niu, X. Wang, F. Yi, Y.S. Zhou, Z.L. Wang, Nat. Commun. 6 (2015) 8975.
[14] S. Wang, L. Lin, Z.L. Wang, Nano Lett. 12 (2012) 6339–6346.
[15] Z. Zhao, J. Liu, Z. Wang, Z. Liu, W. Zhu, H. Xia, T. Yang, F. He, Y. Wu, X. Fu, L.M. Peng, Nano Energy 41 (2017) 351–358.
[16] X.S. Zhang, M. Su, J. Brugger, B. Kim, Nano Energy 33 (2017) 393–401.
[17] J. Chung, S. Lee, H. Yong, H. Moon, D. Choi, S. Lee, Nano Energy 20 (2016) 84–93.
[18] X.S. Meng, Z.L. Wang, G. Zhu, Adv. Mater. 28 (2016) 668–676.
[19] J.H. Lee, R. Hinchet, S.K. Kim, S. Kim, S.W. Kim, Energy Environ. Sci. 8 (2015) 3605–3613.
[20] P. Basset, E. Blokhina, D. Galayko, Wiley, New York, 2016.
[21] Y. Zi, S. Niu, J. Wang, Z. Wen, W. Tang, Z.L. Wang, Nat. Commun. 6 (2015) 8376.
[22] I.W. Tcho, W.G. Kim, S.B. Jeon, S.J. Park, B.J. Lee, H.K. Bae, D. Kim, Y.K. Choi, Nano Energy 42 (2017) 34–42.
[23] S. Wang, Y. Xie, S. Niu, L. Lin, C. Liu, Y.S. Zhou, Z.L. Wang, Adv. Mater. 26 (2014) 6720–6728.
[24] J. Wang, C. Wu, Y. Dai, Z. Zhao, A. Wang, T. Zhang, Z.L. Wang, Nat. Commun. (2017) 88.
[25] C. Wu, T.W. Kim, H.Y. Choi, Nano Energy 32 (2017) 542–550.
[26] P. Bai, G. Zhu, Y.S. Zhou, S. Wang, J. Ma, G. Zhang, Z.L. Wang, Nano Res. 7 (2014) 990–997.
[27] X. Wen, W. Yang, Q. Jing, Z.L. Wang, ACS Nano 8 (2014) 7405–7412.
[28] X. Chen, M. Han, H. Chen, X. Cheng, Y. Song, Z. Su, Y. Jiang, H. Zhang, Nanoscale 9 (2017) 1263–1270.
[29] T.C. Hou, Y. Yang, H. Zhang, J. Chen, L.J. Chen, Z.L. Wang, Nano Energy 2 (2013) 856–862.
[30] S. Li, J. Wang, W. Peng, L. Lin, Y. Zi, S. Wang, G. Zhang, Z.L. Wang, Adv. Energy Mater. 7 (2017) 1602832.
[31] C. Wu, X. Wang, L. Lin, H. Guo, Z.L. Wang, ACS Nano 10 (2016) 4652–4659.
[32] H. Guo, M.H. Yeh, Y. Zi, Z. Wen, J. Chen, G. Liu, C. Hu, Z.L. Wang, ACS Nano 11 (2017) 4475–4482.
[33] S.L. Zhang, Y.C. Lai, X. He, R. Liu, Y. Zi, Z.L. Wang, Adv. Funct. Mater. 27 (2016) 1606695.
[34] A. Ghaffarinejad, Y. Lu, R. Hichet, D. Galayko, J.Y. Hasani, P. Basset, Electron. Lett. (2017), http://dx.doi.org/10.1049/el.2017.3434.
[35] V. Dorzhiev, A. Karami, P. Basset, F. Marty, V. Dragunov, D. Galayko, IEEE Electron Device Lett. 36 (2015) 183–185.
[36] A. Ghaffarinejad, J.Y. Hasani, R. Hinchet, Y. Lu, H. Zhang, A. Karami, D. Galayko, S.-W. Kim, P. Basset, Nano Energy 1 (2018) accepted.
[37] Y. Lu, E. O'Riordan, F. Cottone, S. Boisseau, D. Galayko, E. Blokhina, F. Marty, P. Basset, J. Micromech. Microeng. 26 (2016) 124004.
[38] R. Hinchet, A. Ghaffarinejad, Y. Lu, J.Y. Hasani, S.W. Kim, P. Basset, Nano Energy 47 (2018) 401–409.
[39] W. Tang, T. Jiang, F.R. Fan, A.F. Yu, C. Zhang, X. Cao, Z.L. Wang, Adv. Funct. Mater. 25 (2015) 3718–3725.
[40] S. Meninger, J.O. Mur-Miranda, R. Amirtharajah, A. Chandrakasan, J.H. Lang, IEEE Trans. Very Large Scale Integr. Syst. 9 (2001) 64–76.
[41] A. Karami, D. Galayko, P. Basset, IEEE Trans. Circuits-I 64 (2017) 227–240.
[42] S. Niu, Y. Liu, Y.S. Zhou, S. Wang, L. Lin, Z.L. Wang, IEEE Trans. Electron Devices 62 (2015) 641–647.
[43] X. Cheng, L. Miao, Y. Song, Z. Su, H. Chen, X. Chen, J. Zhang, H. Zhang, Nano Energy 38 (2017) 438–446.
[44] L. Zheng, G. Cheng, J. Chen, L. Lin, J. Wang, Y. Liu, H. Li, Z.L. Wang, Adv. Energy Mater. 5 (2015).
[45] D. Galayko, A. Dudka, A. Karami, E. O'Riordan, E. Blokhina, O. Feely, P. Basset, IEEE Trans. Circuits-I 62 (2015) 2652–2663.

Hemin Zhang received his B.Eng. degree from Department of Electrical Engineering and Automation in 2011, and the Ph.D. degree from the MOE Key Laboratory of Micro and Nano Systems for Aerospace in 2017, both in Northwestern Polytechnical University, Xi'an, China. He is currently a postdoc in Universit'e Paris-Est, ESYCOM Lab., ESIEE Paris. His research interests include mode-localized resonant MEMS sensors and triboelectric nanogenerator. He was a recipient of the Transducer 2015 Outstanding Paper Finalist Award and the MEMS 2016 Outstanding Paper Award Winner.

Yingxian Lu is a Ph.D. student under the co-supervision of Professor Philippe Basset and JeanMarc Laheurte at ESYCOM lab, Université Paris-Est. Her research interests include kinetic energy harvesters for power supply applications of wireless sensor nodes or for wearable electronics, MEMS device modeling, design and characterization, RF system optimization, and flexible electronic devices. Her research is focused on capacitive kinetic energy harvesters working with ultra-low frequency vibrations or motions, including random environmental vibrations, machine vibrations, or human motions.

Ali Ghaffarinejad is pursuing his Ph.D. degree in electrical engineering at School of Electrical Engineering, Iran University of Science and Technology (IUST), Tehran, Iran. He received his B.Sc. degree in electronics engineering from the University of Kerman, Iran, in 2006, the M.Sc. degree in Biomedical engineering from IUST in 2011. He is currently a visiting student at ESYCOM lab, Université Paris-Est/ ESIEE, Paris, France. His research interests include study of triboelectric charge transfer and induction through rough surfaces, design and modeling of RF-MEMS devices. He focus on the modeling and characterization of triboelectric transducers and interface circuits for mechanical energy harvesters.

Dr. Philippe Basset is professor at Université Paris-Est / ESIEE Paris. He received his Ph.D. from IEMN / University of Lille in 2003 in the areas of microelectronic and microelectromechanical-systems (MEMS). In 2004 he was a postdoc at CMU, Pittsburgh, USA and he joined ESIEE Paris in 2005. His current research interests include micro-power sources for autonomous MEMS and micro/nano-structuration of silicon. He serves in the International Steering Committee of the PowerMEMS conference since 2015. Member of the ESYCOM laboratory, he is currently leading the Sensors and Measuring MEMS group.